Reprinted with permission from
JOURNAL OF CARDIOVASCULAR ELECTROPHYSIOLOGY, Volume 12, No. 6, June 2001

Experimental and Theoretical Analysis of Phase Singularity Dynamics in Cardiac Tissue

MARK-ANTHONY BRAY, M.S.E., SHIEN-FONG LIN, PH.D.,* RUBIN R. ALIEV, PH.D.,* BRADLEY J. ROTH, PH.D.,† and JOHN P. WIKSWO, JR., PH.D.*

From the Departments of Biomedical Engineering and *Physics and Astronomy, Vanderbilt University, Nashville, Tennessee; and the †Department of Physics, Oakland University, Rochester, Michigan

Phase Singularity Dynamics. ***Introduction:*** **Quantitative analysis of complex self-excitatory wave patterns, such as cardiac fibrillation and other high-order reentry, requires the development of new tools for identifying and tracking the most important features of the activation, such as phase singularities.**

Methods and Results: **Image processing operations can be used to detect the phase singularity at the tip of a spiral wave. The phase space behavior of a spatiotemporal sequence of data may be reconstructed using time-series analysis. The phase singularities then are localized efficiently by computing the topologic charge density as the curl of the spatial phase gradient. We analyzed the singularity interaction dynamics of both experimentally observed and numerically simulated instances of quatrefoil reentry and found that the singularity behavior in the experimental preparations can be classified into three categories on the basis of how their separation changes with time.**

Conclusion: **Topologic charge densities can be calculated easily and efficiently to reveal phase singularity behavior. However, the differences between theoretical and experimental observations of singularity separation distances indicate the need for more sophisticated numerical models.** *(J Cardiovasc Electrophysiol, Vol. 12, pp. 716-722, June 2001)*

nonlinear dynamics, arrhythmia, phase singularity, topologic charge, optical imaging, cardiac reentry

Introduction

Reentrant excitation, a phenomenon in which a wave of excitation repeatedly activates the same area of tissue independently of the natural cardiac rhythm, is believed to play a significant role in the initiation of lethal arrhythmias, such as ventricular tachycardia and fibrillation.[1,2] The reentrant circuit around which activation propagates can be defined by an anatomic obstacle, such as an infarction, or by heterogeneities of dynamic electrical properties of normal cardiac tissue, such as the time course of repolarization and recovery of excitability.[3,4] Under such circumstances, the circuit can manifest itself in the form of spiral waves.[5] These waves may remain stationary, drift, and even give rise to multiple, dynamic reentrant pathways.[6,7] The quantitative analysis of these complex spatiotemporal patterns of activation requires the development of new tools that allow for identifying and tracking the most important topologic features of the patterns. Simple excitatory waves in nonlinear dynamic systems, such as the spiral wave in the Belousov-Zhabotinsky (BZ) reaction[8] or in cardiac tissue, typically are analyzed by comparing experimental observations with the theoretical predictions of numerical models.[9]

The spiral wave rotates about an organizing center, or core, which is thought to be an unexcited but excitable medium that defines the primary dynamic characteristics of the wave.[10,11] Within the core, there is a phase singularity, i.e., a region where the phase is undefined. The phase singularity may be described in terms of topologic charge, n_t,[12,13] defined as given in Equation 1:

$$n_t \equiv \frac{1}{2\pi} \oint_c \nabla\phi \cdot d\vec{l}, \tag{1}$$

where $\phi(\vec{r})$ is the local phase, and the line integral is taken over path $\vec{l}$ on a closed curve c surrounding the topologic defect. Even though the core cannot be easily distinguished from the surrounding active tissue, it is possible to observe and track the phase singularity. Hence, it is upon this element that we focus our attention.

Methods

Theoretical studies of self-excitatory systems can examine the relationship of the pair of key excitatory and recovery variables in phase space, in which one variable is plotted against the second. In experimental studies, there is typically a single observable variable, such as the transmembrane potential in cardiac tissue, which we will call $V(\vec{r},t)$. To allow us to analyze the system in phase space, we use time-series analysis to create a second variable, $V'(\vec{r},t)$, which is defined by time delay embedding of V:

$$V'(\vec{r}, t) \equiv V(\vec{r}, t + \tau), \tag{2}$$

where τ is the delay calculated as the first zero crossing of the autocorrelation of $V(\vec{r},t)$, indicating linear independence.[14] From these two variables, we can represent the temporal behavior of an excitable element in phase space as

This work has been supported by National Institutes of Health Grants R01HL58241 and R01HL57207 and by a National Science Foundation predoctoral fellowship to M-A. Bray.

Address for correspondence: Mark-Anthony Bray, M.S.E., Department of Biomedical Engineering, Vanderbilt University, 5824 Stevenson Center, Nashville, TN 37235. Fax: 615-343-7919; E-mail: mark.bray@vanderbilt.edu

Manuscript received 25 October 2000; Accepted for publication 23 March 2001.

a closed path, termed a phase trajectory. We then can define the local phase of this element, $\phi(r,t)$, in terms of angle, around the trajectory in phase plane, referenced to a central point.

By defining the integrand of Equation 1, the gradient of the phase, as a wave vector, $\vec{k}$,

$$\vec{k}(\vec{r}, t) \equiv \nabla\phi(\vec{r}, t) = \frac{\partial}{\partial x}\phi(\vec{r}, t)\hat{\imath} + \frac{\partial}{\partial y}\phi(\vec{r}, t)\hat{\jmath}, \quad (3)$$

we see that by evaluating n_t for a small circular path of radius a in Equation 1, the topologic charge n_t is proportional to the curl of the wave vector. Specifically, we are concerned with the component perpendicular to the plane containing c:

$$(\nabla \times \vec{k}) \cdot \hat{z} \equiv \lim_{a \to 0} \frac{1}{\pi a^2} \oint_c \vec{k} \cdot d\vec{l}. \quad (4)$$

where $\vec{k}$ and $d\vec{l}$ are assumed to be restricted to the xy plane. Because $\vec{k}$ is derived from the gradient of a scalar field, the curl of $\vec{k}$ is zero everywhere where ϕ is differentiable, except at the phase singularity itself, where ϕ is undefined. This integral may be computed by the following procedure. The wave vector $\vec{k}$ may be approximated from a discretized phase image consisting of pixels $\phi[m,n]$ by a finite difference operation in the x and y directions:

$$k_x[m, n] = \nabla\phi_x[m, n] = \phi[m + 1, n] - \phi[m, n] \quad (5)$$

$$k_y[m, n] = \nabla\phi_y[m, n] = \phi[m, n + 1] - \phi[m, n]. \quad (6)$$

Absolute phase jumps greater than π in adjacent elements are corrected by converting them to their 2π complement. Computation of the line integral in Equation 1 at location $[m,n]$ may be expressed as a convolution operation:

$$(\nabla \times \vec{k}) \cdot \hat{z} \propto \nabla_x \otimes k_y + \nabla_y \otimes k_x, \quad (7)$$

where $\otimes$ is the convolution operator, and

$$\nabla_x = \begin{bmatrix} -1/2 & 0 & +1/2 \\ -1 & 0 & +1 \\ -1/2 & 0 & +1/2 \end{bmatrix}, \text{ and}$$

$$\nabla_y = \begin{bmatrix} +1/2 & +1 & +1/2 \\ 0 & 0 & 0 \\ -1/2 & -1 & -1/2 \end{bmatrix} \quad (8)$$

are the convolution kernels.

The procedure developed here was used to locate phase singularities within a fourfold symmetric reentrant pattern known as quatrefoil reentry.[15,16] Such a pattern was demonstrated recently in cardiac tissue, and, in contrast to most reentrant arrhythmias, it can be used to create repeatable patterns of four closely interacting singularities. In this article, we analyze data from our earlier experiments. The experimental protocol was described previously,[16] but we summarize it here briefly. High-speed optical imaging using a CCD camera at 267 frames/sec was used to record the response of five isolated, Langendorff-perfused rabbit hearts stained with the voltage-sensitive dye di-4-ANEPPS. The calcium channel antagonist D600 (1 μM) was added to the perfusate to inhibit motion artifacts. A premature S2 cathodal stimulus was delivered within the vulnerable phase during periodic pacing via a unipolar point electrode placed on the posterior left ventricle. Within a narrow range of coupling intervals, the boundary between the induced virtual anodes and virtual cathodes provided four pathways by which reentry could occur after the termination of the S2 stimulus. Although the resultant quatrefoil reentry was not sustained, lasting only a few cycles, there was sufficient propagation to clearly identify the reentrant pattern. Spatial and temporal filtering was applied to improve the signal-to-noise ratio, and the signals were normalized with respect to the S1 amplitude. The value of τ used for a spatiotemporal data sequence was calculated as the average of the optimal values of τ calculated for each pixel in that sequence.

Results

The earlier work by Gray et al.[14] and our present study are the first to provide quantitative, experimental measurements of the interaction dynamics of multiple singularities in cardiac tissue. Although Gray et al. tracked as many as four singularities at one time and could observe singularity annihilation, the dynamics of the interaction between these singularities was not analyzed. In contrast, our experimental and theoretical studies of quatrefoil reentry provide us with the requisite data required to test our understanding of these interactions. For this study, the tissue was modeled as an anisotropic bidomain, both as a two-dimensional (2D) sheet of tissue and a three-dimensional (3D) cylinder of tissue, using cylindrical coordinates (z,ρ,θ) to specify position; axisymmetry allowed the results for the cylinder to be determined independently of θ by means of an appropriate coordinate transformation. The active membrane components were modeled using Beuler-Reuter kinetics, slightly modified such that strong hyperpolarization would not produce unrealistic membrane conductance, and the speed of the calcium channel kinetics increased by a factor of eight to ensure a stable spiral wave. Further details on the model parameters are described elsewhere.[17] Figure 1 shows the spatiotemporal pattern described by quatrefoil reentry for both a numerically simulated model and an experimental preparation. Both groups of data were normalized to unity with respect to the S1 stimulus.

Previous studies indicated that a reduced variation in action potential amplitude exists in those regions that either are undergoing conduction block or are located within the core of a spiral wave.[5,16] It stands to reason that calculating the variance of sequential, overlapping segments of the temporal signal and identifying those regions of low variance will highlight these areas. Figure 2 shows the spatiotemporal relationship between the motion of the activation wave and the regions of low variance shortly after initiation of quatrefoil reentry for both the numerical model and experimental preparation. In each instance, the black mesh encloses the low-variance regions calculated with an isovalue of 0.2 in Figure 2A and 0.06 in Figure 2B. The presence of four distinct low-variance regions and the fact that the colored surface representing the wavefront rotates around each of the meshes confirms that the phase singularity should be located within the low-variance region.

Figure 3 shows a comparison between numerical simulation and experimental preparations of quatrefoil reentry, along with the images after application of the phase and curl

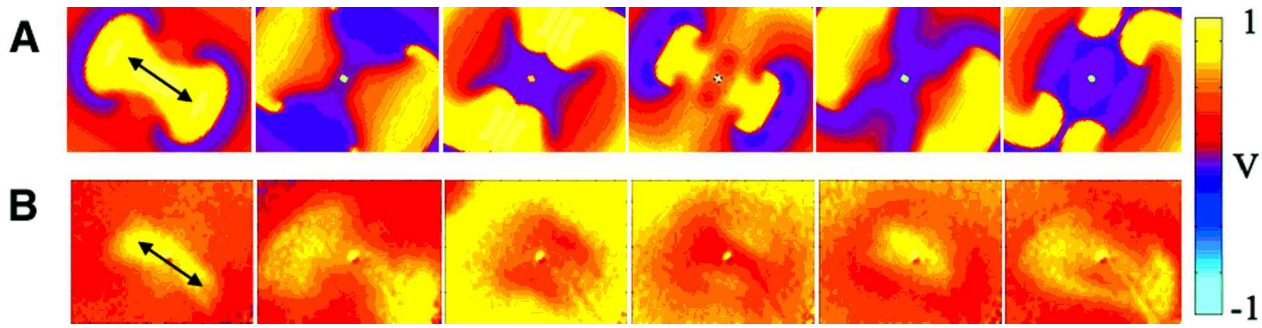

Figure 1. *Spatiotemporal distribution during quatrefoil reentry of the (A) transmembrane potential in a numerically simulated model and (B) fluorescence intensity in an experimental preparation. The fluorescent signal obtained from the epicardium is proportional to the transmembrane potential. The color bar indicates the pseudocolors used for representing the normalized signal magnitude: yellow is fully depolarized, blue is hyperpolarized, and purple is resting. Arrow indicates fiber direction.*

operations. The calculated values of τ were on the order of 26 msec for the experimental data sequences and 35 msec for the numerically simulated datasets. In Figures 3B and 3C, note the presence of four phase singularities. In particular, the value of the curl at the singularity positions in Figure 3C corresponds to the spiral wave chirality (blue corresponds to clockwise rotation, red to counterclockwise). Thus, by this method, we succeeded in isolating the phase singularity of spiral waves for analysis. Figure 4 shows an example of quatrefoil trajectories obtained from application of the above algorithm to both experimentally prepared and numerically simulated data. It can be seen clearly that the singularities exhibit dynamic behavior.

In 3D figure-of-eight reentry, the symmetry of the system requires that the two singularities define the ends of a filament about which the single scroll wave rotates. In the instance of quatrefoil reentry, the observed surface pattern is consistent with two pairs of phase singularities connected by two singularity filaments, about which a pair of synchronized scroll waves rotates underneath the epicardial surface. If we consider the finite thickness of the left ventricular wall, the possibility of two transmural filaments cannot be

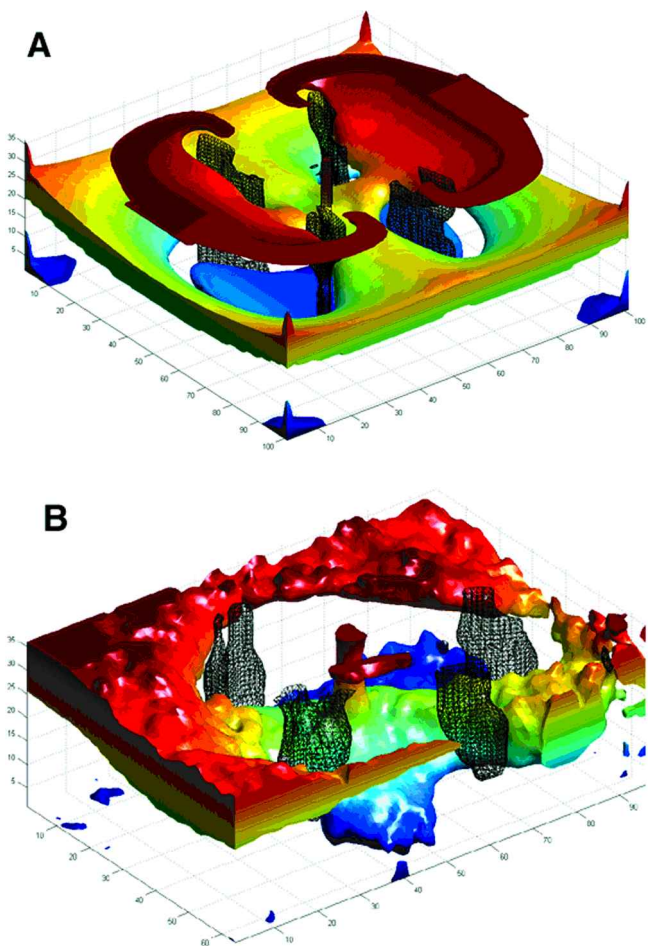

Figure 2. *Spatiotemporal evolution of a quatrefoil reentrant wavefront pattern relative to regions of low variance of wavefront amplitude in (A) numerically simulated and (B) experimental preparations. Spatial axes lies in the horizontal plane; temporal axis is vertical. Solid surface represents isopotential surface of the reentrant wavefront where the normalized V_m is 0.7, colored for clarity. Black mesh encloses regions of reduced variance in temporal signal, calculated at a threshold variance value of 0.2 (A) and 0.06 (B).*

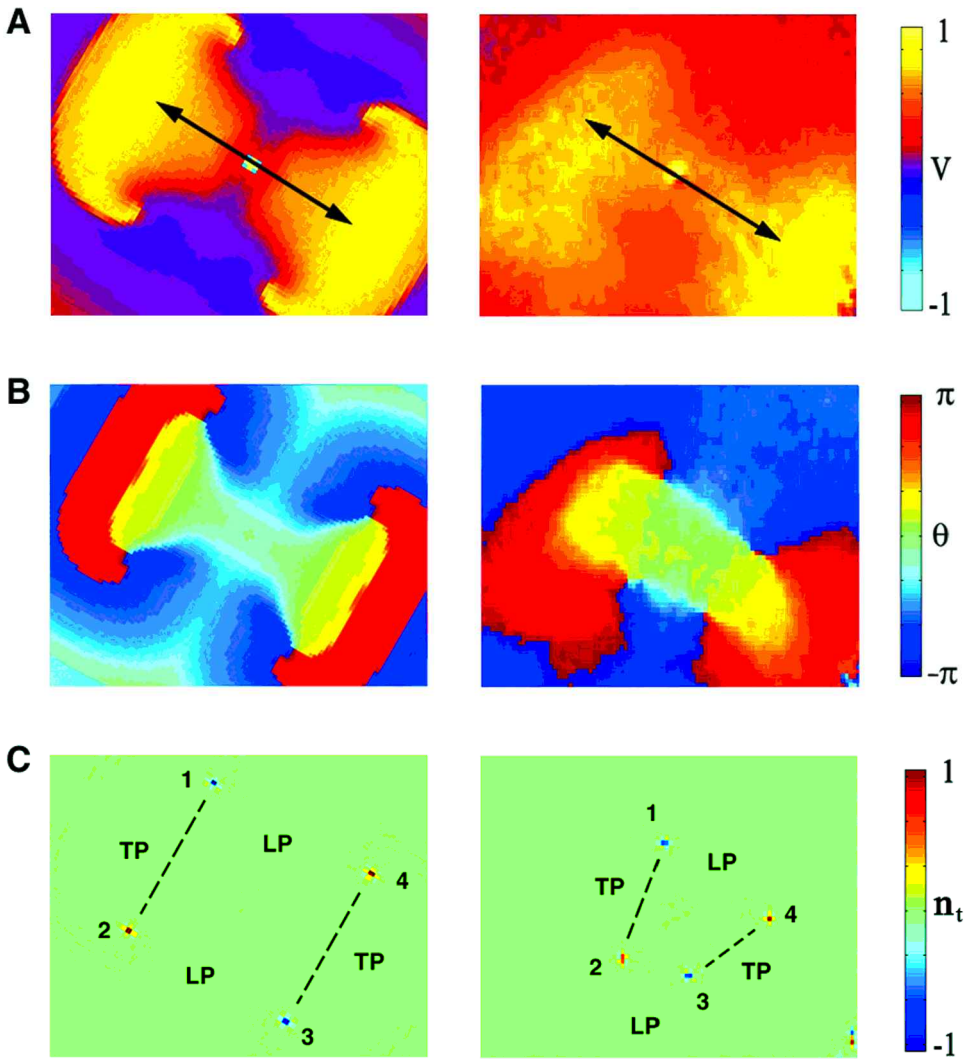

Figure 3. *Numerically simulated (left column) and experimental (right column) quatrefoil reentry following an electrical stimulus applied to the center of tissue. (A) Normalized spatial distribution of transmembrane potential from simulated data and fluorescence intensity from experimental data. Arrow indicates fiber direction. (B) Phase distribution of image in panel A. (C) Curl distribution of wave vectors calculated from image in panel B, highlighting the presence of four phase singularities. Transverse pairs (TP) are indicated by numbers 1 and 2, and 3 and 4; longitudinal pairs (LP) are indicated by numbers 1 and 4, and 2 and 3.*

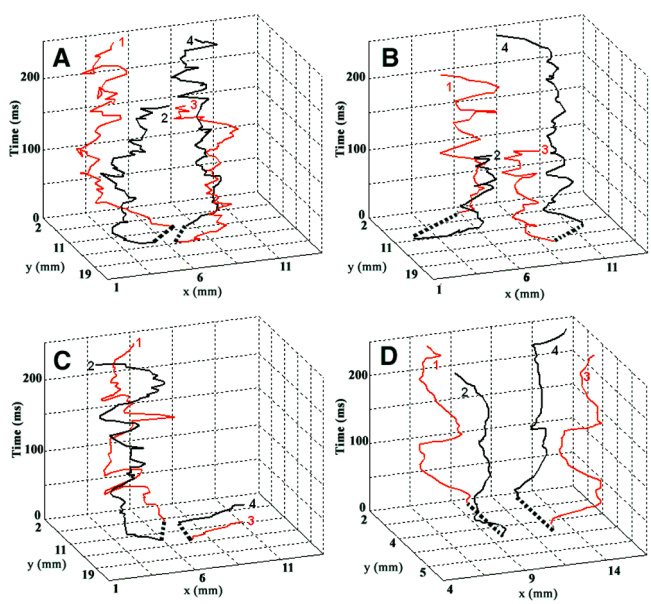

Figure 4. *Trajectories of quatrefoil phase singularities in x, y, t space, illustrating dynamic behavior in time. The singularities are numbered 1 to 4 and connected in the same order as in Figure 3, to indicate transverse pairs and longitudinal pairs. Time interval is measured from the end of the S2 stimulus. (A) Type I: initial linear expansion followed by linear contraction; (B) type II: initial linear contraction followed by oscillatory contraction; (C) type III: initial linear expansion followed by expansion trend; (D) 3D numerical model pair separation distances.*

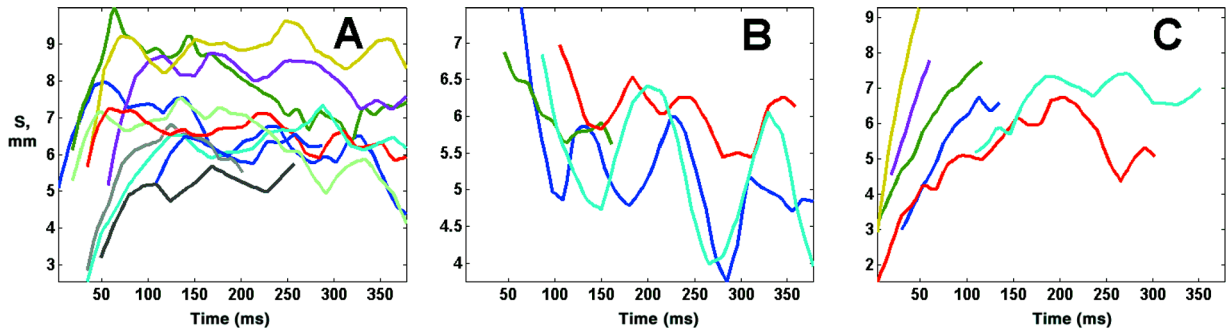

Figure 5. *Plots of the average of the transverse pair and longitudinal pair separation distances for all instances of quatrefoil reentry grouped into the three types. Each curve represents a different experiment. (A) Type I; (B) type II; (C) type III.*

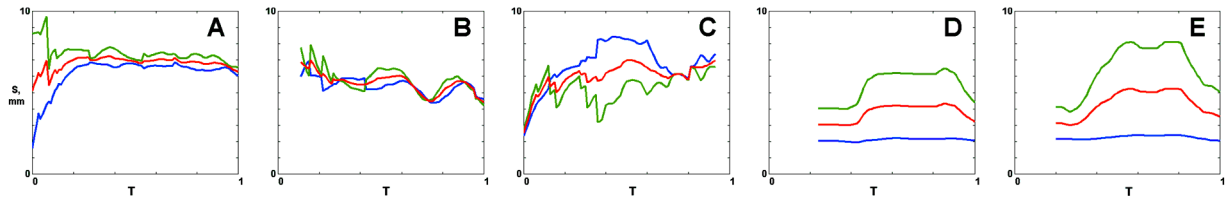

Figure 6. *Taxonomy of the pair separation distance S (in mm) plotted as a function of time T, computed as a fraction of the rotation period. T = 0 represents the termination of the S2 stimulus. Blue, green, and red lines represent transverse pair, longitudinal pair, and average separation distances, respectively. Curves begin from time of first detection of singularities. (A) Type I; (B) type II; (C) type III; (D) 2D numerical model pair separation distances; (E) 3D numerical model pair separation distances.*

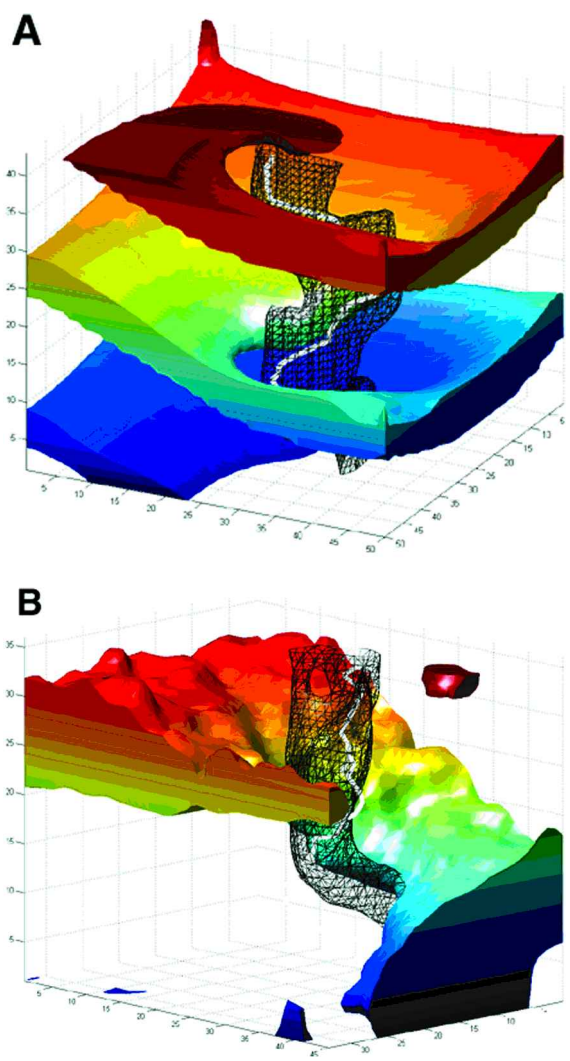

Figure 8. *Spatiotemporal evolution of a single spiral wave from Figure 2 relative to region of low variance of wavefront amplitude and phase singularity trajectory in (A) numerically simulated and (B) experimental preparations. Spatial axis lies in the horizontal plane; temporal axis is vertical plane. Solid surface represents isopotential surface of the reentrant wavefront where the normalized V_m is 0.7, colored for clarity. Black mesh encloses regions of reduced variance in temporal signal, calculated at a threshold variance value of 0.2 (A) and 0.06 (B). Thick white line represents trajectory of the phase singularity.*

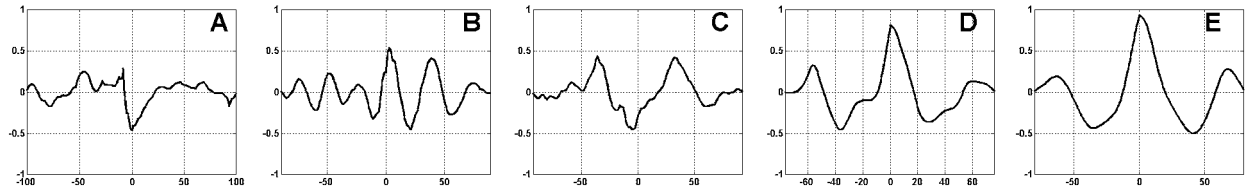

Figure 7. *Cross-correlation of transverse pair and longitudinal pair separation distances. (A) Type I; (B) type II; (C) type III; (D) 2D numerical model; (E) 3D numerical model.*

ruled out conclusively. For this article, we define the term *transverse pair* (TP) as the oppositely charged singularity pair aligned perpendicular to the axis of symmetry defined by the cardiac fiber direction, as shown in Figure 3A. A *longitudinal pair* (LP) describes the pair of singularities aligned parallel to the cardiac fiber axis of symmetry. Examples of TP and LP are illustrated in experimental and simulated data in Figure 3C.

We examined relative distances between transverse and longitudinal singularity pairs for 20 cases of quatrefoil reentry. For the earliest detectable singularities, in the majority of cases the TP separation was less than that of the LP separation. We found that TP and LP exhibit dynamic behavior that could be grouped into three classifications on the basis of the time course of the average pair separation, as shown by specific examples of trajectories in Figure 4. The average of the TP and LP separation distances for each of the 20 instances of quatrefoil reentry is shown in Figure 5. Figure 6 shows the TP and LP separation distances, along with the average of the TP and LP separation distances, averaged for each classification. The taxonomy of the separation distances is described as follows:

1. Type I (n = 10) is characterized by an initial expansion in the TP separation distance and a contraction in the LP separation distance to form a more equidistant arrangement in the four singularities. The initial phase has an average expansion velocity of 0.20 mm/msec. Both pairs then exhibit weak oscillatory behavior at a relatively constant separation distance (Figs. 4A, 5A, and 6A).
2. Type II (n = 4) is characterized by an initial overall contraction in both TP and LP separation distance, with an average contraction velocity of 0.30 mm/msec. Thereafter, both TP and LP separation distances experience strong oscillatory behavior, coupled with a contraction in separation distance (Figs. 4B, 5B, and 6B).
3. Type III (n = 6) is characterized by an initial overall expansion in both TP and LP separation distances, with an average expansion velocity of 0.83 mm/msec. Afterward, both pairs exhibit oscillatory behavior with an expanding trend in separation distance. At times, the average TP separation is less than half that of the average LP separation (Figs. 4C, 5C, and 6C).

Several interesting observations may be made based on Figure 4. Note that in Figure 4C, a TP is the first to extinguish (labeled 3 and 4). However, in Figures 4A and 4B, the LP singularities labeled 2 and 3 are extinguished in both cases, most likely by mutual annihilation in the instance of Figure 4A, on the basis of their proximity at the time the singularities disappear. This behavior in Figures 4A and 4B suggests that the filament remnants of 1 and 4 have either spanned the myocardial wall so that the other end of the filament is not visible or recombined to form a new transverse pair.[18]

The same calculations were applied to the numerically simulated data. In comparison, analysis of pair separation for the model datasets did not conform to any of the three classifications, exhibiting clearly repetitive oscillatory behavior for both TP and LP, in both the 2D and 3D cases. Examples of numerically simulated separation distances are shown in Figures 6D and 6E.

Examination of the periodicity of interaction between the singularities was performed by cross-correlating the TP and LP separation distances, as shown in Figure 7. As indicated earlier, the oscillatory nature of type II behavior is reflected in the cross-correlation (Fig. 7B), which indicated a period of oscillation of 133 msec. Type III also suggested an oscillation of separation distances (Fig. 7C), albeit over a wider period, unlike type I, which exhibited no interdependence of separation distances (Fig. 7A). The cross-correlations for the numerical models both display a strong correlation at the zero-th shift.

Discussion

Now that we have identified the phase singularities and can compute their trajectory in physical space, we can return to Figure 2 and compare the trajectory to the regions of low variance. Figure 8 shows a single spiral wave from the quatrefoil reentry with the corresponding phase singularity trajectory overlaid as a white line. Although the mesh encloses the trajectory completely in the numerical model (Fig. 8A), for the instance of the experimental preparation, the trajectory may wander outside the mesh at some places (Fig. 8B). Whether this disparity is due to the rapidity of singularity motion, the width of the overlapping temporal segments used to calculate variance, or the calculation of phase itself is a topic of further research. In both cases, we see that the phase singularity trajectory follows the time course of the low-variance mesh, as expected.

The interaction of rotors has been discussed intensively in the literature,[19-21] but the problem is far from being resolved. Analytical solutions have been found for simple systems such as those governed by the Ginzburg-Landau equations,[22,23] demonstrating that inhomogeneities within the medium will cause frequency-dependent spiral wave interaction. For systems with FitzHugh-Nagumo dynamics, no analytical solution has yet been found; numerical simulations show the oscillatory interaction of vortices at close range where the parameter values have been constrained to prohibit single vortex meander,[24] a significant difference from experimental observations.[6,7] The long-range interaction of vortices has been studied in the BZ reaction,[25] again indicating a frequency-dependent element involved in vor-

tex drift. At short distances, it was established experimentally that vortices with opposite topologic charges can annihilate,[14] in accordance with theory.[13]

In this article, we observed a significant difference in the singularity dynamics (as defined as the time dependence of the singularity separation distance) between the experimental preparations and numerical models. One possible source of this discrepancy may be the addition of the excitation decoupler D600 to suppress mechanical contractions for the purposes of the experiment. Electromechanical uncoupling agents have been used previously for the purpose of optical mapping of phase singularities.[14] D600 is known to alter wavefront dynamics, but its full range of effects on singularity dynamics cannot be determined without further study beyond the scope of this initial article.

Current evidence supports the dependence of epicardial phase singularity dynamics on underlying filament behavior.[7] Further exploration into the correlation of experimental and numerical results will necessitate the development of more detailed models. A future step is to carry out numerical simulations of filament behavior in a 3D model of continuous myocardium that more closely represents the physiologic substrate that may be found in experimental preparations. Another issue that needs to be addressed is the fact that using time-series analysis is but one of several techniques to calculate phase for an oscillatory system (for review, see Pikovsky et al.[26]). The algorithm described here is designed to detect a 2π phase change around a point, regardless of the technique used to generate the spatial distribution of phase values. However, the influence of the method chosen to construct the phase map on phase singularity localization (and the derived dynamics) is not yet fully understood.

Conclusion

The concept of topologic charge provides a technique to localize phase singularities easily and efficiently present in cardiac tissue that is undergoing reentrant excitation to reveal the dynamics of their behavior. Our experimental study demonstrates both expansion and contraction of the distance between singularities and annihilation of singularities that are either connected by a filament or not. We conclude that the experimentally observed dynamics are more complex and varied than those predicted by our model, because the dynamic properties of the model are too simple, the anisotropies and heterogeneities of the tissue are not adequately represented, or the model is not operating in the correct parameter space. Until the models are improved, our experimental observations of quatrefoil reentry provide us with an excellent, although experimentally challenging, system for the study of singularity dynamics.

Acknowledgments: We are indebted to Richard Gray and Alan Garfinkel for their comments and suggestions.

References

1. Mines GR: On circulating excitations in heart muscles and their possible relation to tachycardia and fibrillation. Trans R Soc Can 1914;4:43-52.
2. El-Sherif N: Reentrant mechanisms in ventricular arrhythmias. In Zipes DP, Jalife J, eds: *Cardiac Electrophysiology: From Cell to Bedside.* Second Edition. WB Saunders, Philadelphia, 1995, pp. 567-582.
3. Allessie MA, Bonke FIM, Schopman FJG: Circus movement in rabbit atrial muscle as a mechanism of tachycardia: I. Circ Res 1973;23:54-62.
4. Hoffman BF, Rosen MR: Cellular mechanism for cardiac arrhythmias. Circ Res 1981;49:1-15.
5. Pertsov AM, Davidenko JM, Salomonsz R, Baxter WT, Jalife J: Spiral waves of excitation underlie reentrant activity in isolated cardiac muscle. Circ Res 1993;72:631-650.
6. Davidenko JM, Pertsov AM, Salomonsz R, Baxter WP, Jalife J: Spatiotemporal irregularities of spiral wave activity in isolated ventricular muscle. J Electrocardiol 1992;24(Suppl):113-122.
7. Gray RA, Jalife J, Panfilov A, Baxter WT, Cabo C, Davidenko JM, Pertsov AM: Nonstationary vortexlike reentrant activity as a mechanism of polymorphic ventricular tachycardia in the isolated rabbit heart. Circulation 1995;91:2454-2469.
8. Zaikin AN, Zhabotinsky AM: Concentration wave propagation in two-dimensional liquid-phase self-oscillating system. Nature 1970; 225:535-537.
9. Winfree AT: *When Time Breaks Down: The Three-Dimensional Dynamics of Electrochemical Waves and Cardiac Arrhythmias*. Princeton University Press, Princeton, NJ, 1987.
10. Ikeda T, Uchida T, Hough D, Lee JJ, Fishbein MC, Mandel WJ, Chen P-S, Karagueuzian HS: Mechanism of spontaneous termination of functional reentry in isolated canine right atrium. Evidence for the presence of an excitable but nonexcited core. Circulation 1996;94: 1962-1973.
11. Zykov VS: *Simulation of Wave Processes in Excitable Media.* Manchester University Press, Manchester, 1987.
12. Goryachev A, Kapral R: Spiral waves in chaotic systems. Phys Rev Lett 1996;76:1619-1622.
13. Mermin ND: The topological theory of defects in ordered media. Rev Mod Phys 1979;51:591-648.
14. Gray RA, Pertsov AM, Jalife J: Spatial and temporal organization during cardiac fibrillation. Nature 1998;392:75-78.
15. Roth BJ, Lin S-F, Wikswo JP Jr: Unipolar stimulation of cardiac tissue. J Electrocardiol 1998;31(Suppl):6-12.
16. Lin S-F, Roth BJ, Wikswo JP Jr: Quatrefoil reentry in myocardium: An optical imaging study of the induction mechanism. J Cardiovasc Electrophysiol 1999;10:574-586.
17. Roth BJ: Nonsustained reentry following successive stimulation of cardiac tissue through a unipolar electrode. J Cardiovasc Electrophysiol 1997;8:768-778.
18. Fenton F, Karma A: Fiber-rotation-induced vortex turbulence in thick myocardium. Phys Rev Lett 1998;81:481-484.
19. Krinsky VI, Agladze KI: Interaction of rotating waves in an active chemical medium. Physica D 1983;8:50-56.
20. Wu X-G, Chee M-N, Kapral R: Vortex dynamics in oscillatory chemical systems. Chaos 1991;1:421-434.
21. Aranson IS, Kramer L, Weber A: On the interaction of spiral waves in non-equilibrium media. Physica D 1991;53:376-384.
22. Hagan PS: Spiral waves in reaction-diffusion equations. SIAM J Appl Math 1982;42:762-786.
23. Hendrey M, Ott E, Antonsen TM Jr: Effect of inhomogeneity on spiral wave dynamics. Phys Rev Lett 1999;82:859-862.
24. Ermakova EA, Pertsov AM, Shnol EE: On the interaction of vortices in two-dimensional active media. Physica D 1989;40:185-195.
25. Aliev RR, Davydov VA, Toshinori K, Yamaguchi T: Long range interaction of vortices in a chemical active medium. Netsu Sokutei 1997;24:194-198.
26. Pikovsky AS, Rosenblum MG, Osipov GV, Kurths J: Phase synchronization of chaotic oscillators by external driving. Physica D 1997; 104:219-238.